Article type: Original Paper

Breaking Malus' Law: Highly Efficient, Broadband, and Angular Robust Asymmetric Light Transmitting Metasurface

*Cheng Zhang[1], Carl Pfeiffer[1], Taehee Jang[1], Vishva Ray[2], Maxwell Junda[3], Prakash Uprety[3], Nikolas Podraza[3], Anthony Grbic[1] and L. Jay Guo[1]**

*Corresponding Author: guo@umich.edu

[1]Department of Electrical Engineering and Computer Science, University of Michigan, Ann Arbor, Michigan 48109, USA

[2]Lurie Nanofabrication Facility, Department of Electrical Engineering and Computer Science, University of Michigan, Ann Arbor, Michigan 48109, USA

[3]Department of Physics and Astronomy & Wright Center for Photovoltaics Innovation and Commercialization, University of Toledo, Ohio, 43606, USA

ABSTRACT:

High efficiency, broad bandwidth, and robust angular tolerance are key considerations in photonic device design. Here, a few-layer, asymmetric light transmitting metasurface that simultaneously satisfies all the above requirements is reported. The metasurface consists of coupled metallic sheets. It has a measured transmission efficiency of 80%, extinction ratio of 13.8 dB around 1.5 μm, and a full width half maximum bandwidth of 1.7 μm. It is as thin as 290 nm, has good performance tolerance against the angle of incidence and constituent nano-structure geometry variations. This work demonstrates a practical asymmetric light transmission device with optimal performance for large scale manufacturing.

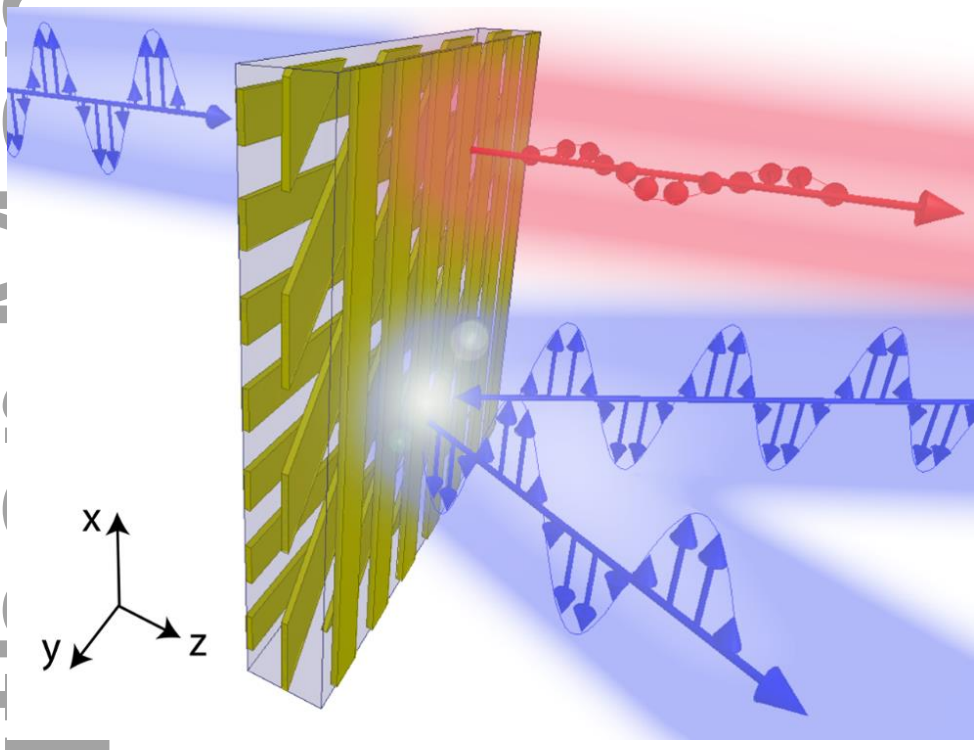

1. Introduction:

Devices providing asymmetric transmission of light are useful components for optical communication systems, information processing, and laser applications [1-4]. Recently, asymmetric light transmission with metamaterials has received considerable interest [5-8]. Although these devices are usually reciprocal and not suitable for applications such as optical isolation [9, 10], they have unique advantages of passive operation and compact size. They can be realized using photonic crystals [11, 12], helical wires [13], hyperbolic metamaterials [14], coupled nano-antennas [15-17], and non-symmetric gratings [18, 19]. However, they typically suffer from complex fabrication processes, low efficiency, and limited operational bandwidth. For example, helical wires provide efficient and broadband asymmetric transmission for circularly polarized light in the infrared region [13], but they are fabricated by direct laser writing and gold plating, which is complex and time-consuming. Hyperbolic metamaterials sandwiched between two Chromium (Cr) gratings have shown broadband asymmetric light transmission as well, but exhibited a low transmission efficiency [14]. By properly designing the coupling between nano-antennas, researchers have demonstrated asymmetric light transmission [15-17]. But these structures usually require complex fabrication procedures and

precise alignment between the antennas, and their efficiencies need to be further improved. A device consisting of a metallic grating cascaded with a dielectric grating provides close to 100% transmission efficiency in simulation, but has a limited bandwidth [20]. Besides, the performance of these metamaterials is usually sensitive to fabrication errors and the angle of incident light, which limits their practical applications. Further, it is also difficult to employ the same design strategy for asymmetric light transmission at different wavelength ranges.

In this work, we report on a few-layer metasurface offering efficient and broadband asymmetric transmission of light. Metasurfaces are sub-wavelength textured surfaces that can be thought of as the two-dimensional equivalent of metamaterials [21-26]. They exhibit versatile, tailored electromagnetic functions such as frequency selectivity [27, 28], polarization control [29-33], wavefront engineering [34-38], and even nonlinear responses [39-41]. The asymmetric light transmitting metasurface in this work consists of three closely-spaced layers of one-dimensional gold nano-gratings. Contrary to the prediction of conventional theory (e.g., Malus' law), the proper cascade of three layers of nano-gratings instead offers efficient and broadband asymmetric light transmission for linearly polarized light. Furthermore, the device is only 290 nm ($\lambda/5$) thick, and its performance is robust against the angle of incidence and fabrication variations. As an experimental demonstration, a device providing asymmetric transmission at a central wavelength of 1.5 μm is fabricated and characterized, which shows a

transmission efficiency of 80%, extinction ratio of 24:1, and a full width half maximum (FWHM) operating bandwidth of 1.7 μm. Furthermore, the design concept is suitable for large area device manufacturing and can be easily transitioned to achieve asymmetric light transmission at other wavelengths.

2. Experimental Section

The designed asymmetric light transmission metasurface consists of three layers of 40 nm thick gold (Au) nano-gratings, each of which are separated by a 125 nm thick SU-8 dielectric spacer (Figure 1). The nano-gratings on the left and right layers have a period of 140 nm and linewidth of 70 nm. The nano-grating on the middle layer has a period of 200 nm and linewidth of 100 nm. The gratings are oriented 0^{o}, 45^{o}, and 90^{o}, for the first, second, and third layers, respectively.

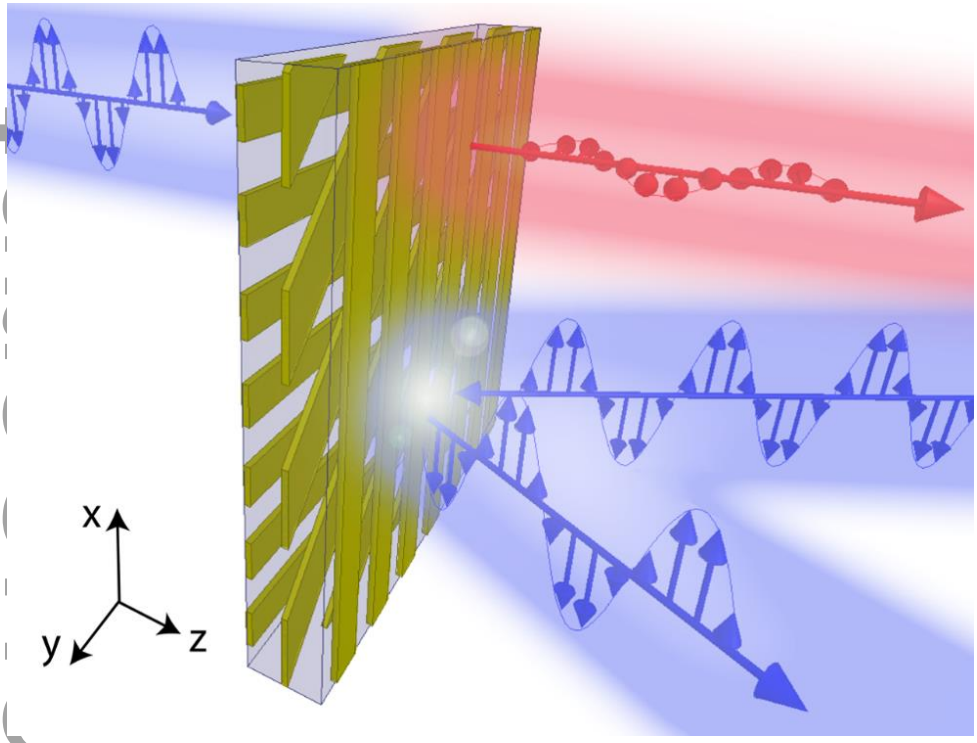

Figure 1: Artistic rendering of the metasurface, consisting of three layers of cascaded Au nano-gratings. The metasurface provides high transmission of x-polarized light incident from the left side, but blocks x-polarized light that is incident from the right side.

The metasurface is fabricated on a 500 μm thick fused silica substrate using the process shown in Figure 2a. The bottom layer is fabricated by electron beam (E-beam) lithography (JEOL 6300FS, JEOL) using Poly(methyl methacrylate) resist (PMMA 950k, A2, Microchem) followed by the deposition of a 3 nm Titanium (Ti) adhesion layer and a 37 nm Gold (Au) layer, and then metal lift-off in an acetone solution. The PMMA layer was spin-coated on the substrate at a rate of 1600 rpm for 40 seconds, and the sample was subsequently baked on the

hotplate at 180 ˚C for 3 minutes. The PMMA thickness was about 100 nm. To solve the charging issues during the E-beam writing, a conductive polymer layer (E-spacer, SHOWA DENKO K.K. 13-9, Shiba Daimon 1-Chome Minato-Ku, Japan) was spin-coated onto the PMMA layer at a rate of 1500 rpm for 45 seconds, and the sample was subsequently baked on the hotplate at 110 ˚C for 2 minutes. The E-spacer layer thickness is about 20 nm. After the E-beam writing, the E-spacer layer was removed after the sample was rinsed in the DI water for 15 seconds. Subsequently, the PMMA layer was developed in the developer solution (1:3 MIBK to IPA) for 45 seconds, and rinsed in IPA for another 30 seconds. To achieve uniform pattern features, proximity effect correction (PEC) was implemented during the E-beam writing. After the metal lift-off, a 125 nm thick SU-8 layer is spun on the metal layer and cured with ultraviolet (UV) radiation (MJB2, Karl Suss). The patterning and metal deposition / lift-off process is repeated three times in order to fabricate all three layers. The scanning electron micrographs (SEMs) of the layers are shown in Figures 2b to 2d.

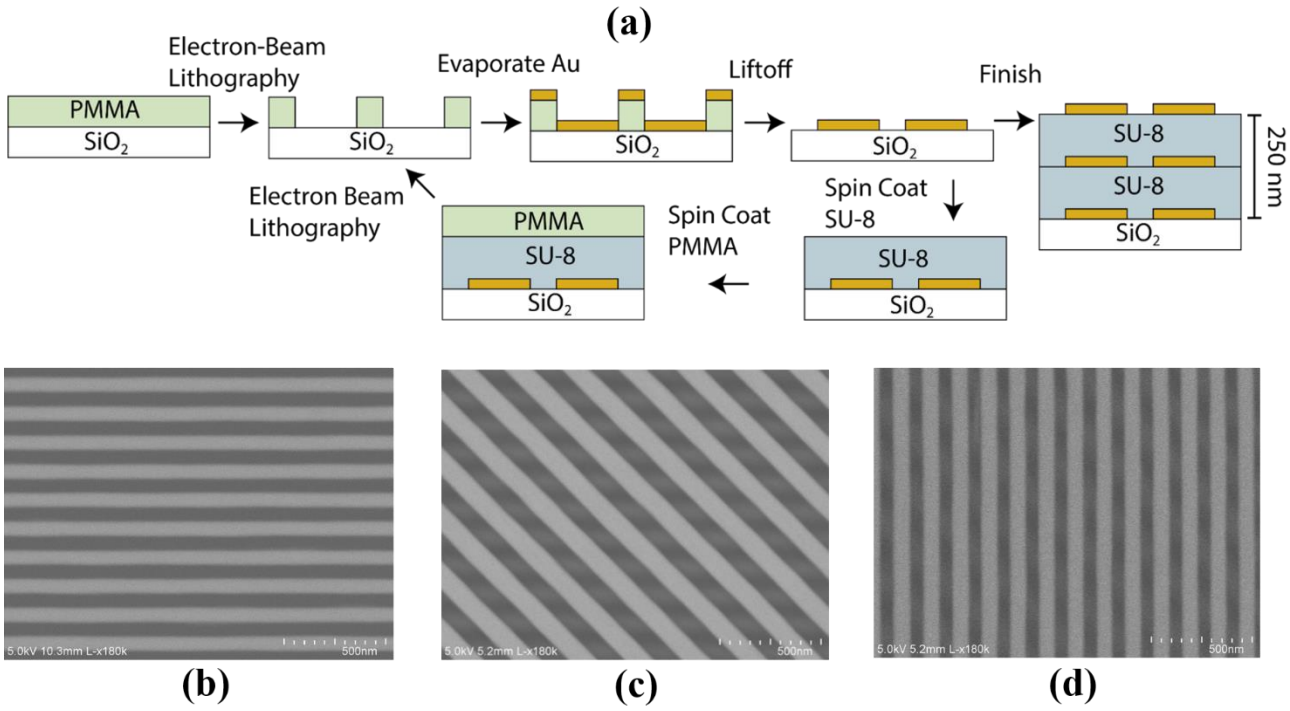

Figure 2: (a) Metasurface fabrication flow chart; (b-d) SEM pictures of the bottom (b), middle (c) and top (d) layer.

The metasurface is experimentally characterized after fabrication. Output from a tunable laser (TLB 6326, Newport, central wavelength at 1.5 μm) is sent through a polarization controller (FPC032, Thorlabs), a single mode optical fiber (P3-1550A-FC-1, Thorlabs), and then onto the metasurface. The polarization state from the input fiber is adjusted by the polarization controller and confirmed by a separate linear polarizer (LPNIRA050-MP2, Thorlabs) before illuminating the metasurface. The light transmitted by the metasurface passes through another linear polarizer (LPNIRA050-MP2, Thorlabs) and is collected by an objective

lens into an optical power meter (2835-C, Newport). The laser wavelength is scanned between 1470 nm and 1530 nm.

3. Results

When x-polarized light is incident from the left side, it is efficiently transmitted through the metasurface and converted to y-polarized output. In contrast, there is very little transmission of x-polarized light when incident from the right (opposite) side of the metasurface. Therefore, this metasurface provides asymmetric transmission for linearly polarized light.

Each layer of the Au nano-gratings individually functions as a linear polarizer, which transmits light polarized orthogonal to the grating, while absorbing/reflecting light polarized along the grating. According to Malus' law, the transmission intensity of a linearly polarized light through a linear polarizer is: $I = I_0 \cos^2 \theta$, where I_0 and I are the light intensity before and after the polarizer, and θ is the angle between the incident light polarization direction and the polarizer transmission axis. In an ideal case where the metallic nano-gratings provide unity light transmission, there will only be 25% transmission intensity for x-polarized light incident from the left side through the cascaded system of three linear polarizers whose transmission axes are rotated 45^o with respect to each other. When the finite cell size and material absorption

are taken into account, the efficiency is even lower. Figure S1 (Supporting Information) plots the product of the Jones matrices for the 3 different layers, which is based on Malus' law and neglects multiple reflections between the layers. The notation T_{nm} means transmission intensity of m-polarized input light into n-polarized output light.

However, Malus' law breaks down for the proposed structure consisting of closely spaced Au gratings. Next, the three layers of cascaded Au nano-gratings are treated as an integrated structure and its electromagnetic response is calculated (linear scale in Figure 3a and logarithmic scale in Figure 3b, see Supporting Information for additional details). In contrast to the predictions of Malus' law, this metasurface provides high transmission of x-polarized light when it is incident from the left side, while blocking the same polarization incident from the right side. The simulated transmission efficiency around 1.5 μm is 85% with an extinction ratio of 53 (17.2 dB). The extinction ratio is defined as the ratio of the transmittance of x-polarized light from the left side ($T_{yx} + T_{xx}$) to the transmittance of x-polarized light from the right side ($T_{xy} + T_{xx}$). The device has a FWHM operating bandwidth of 1.67 μm. Malus' law only applies to cases where the multiple reflections between layers are negligible. However, for the metasurface here, there are strong multiple reflections between the Au nano-grating layers. Such interaction leads to asymmetric light transmission as well as polarization conversion in the structure.

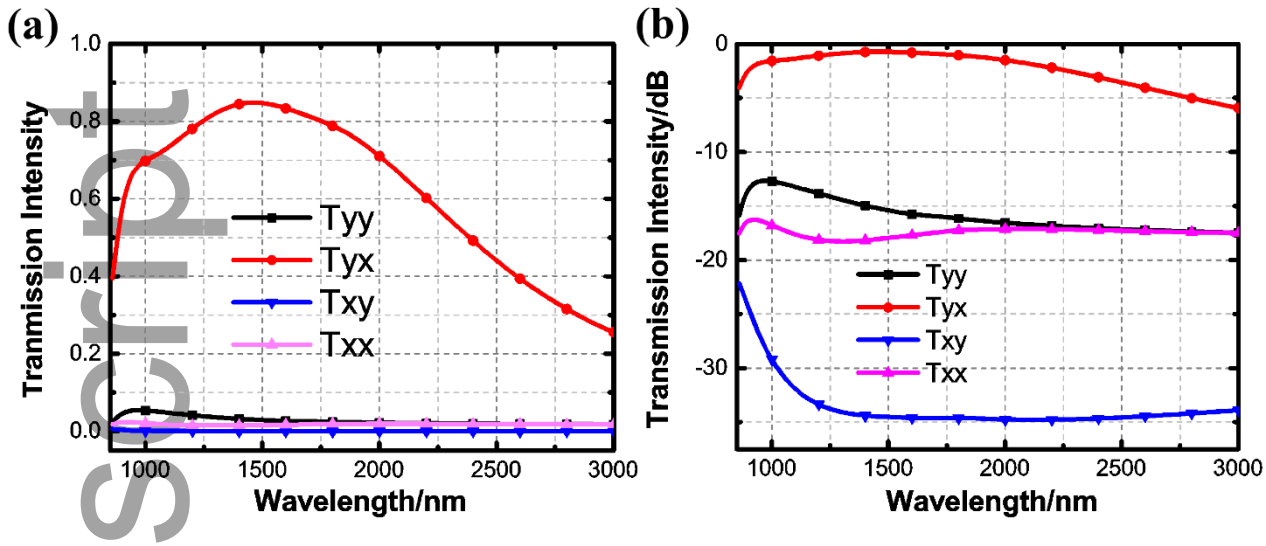

Figure 3: Simulated transmission intensity through the metasurface in linear (a) and logarithmic (b) scale.

The asymmetric response is due to the "cavity effect" rather than the near field coupling between layers. The multiple reflections between layers in this properly designed three-layer structure leads to an enhanced cross-polarization transmittance (T_{yx}) over a broad bandwidth, as well as suppressed transmittances of other co- and cross-polarization conversions (T_{yy}, T_{xy}, and T_{xx}). This leads to the asymmetric light transmission behavior of the metasurface. To better illustrate this point, we have simulated the effective anisotropic impedance of each grating layer first, and then replace the metasurface with three infinitesimally thin sheets which have the effective impedances of the grating layers. In this study, only the "cavity effect" is taken into account. As shown in Figure S2, the simulated transmittance of the three "equivalent sheets" corresponds well with the simulated transmittance of the metasurface.

Cascading two orthogonal 1D metallic gratings (e.g., bottom and top grating layers in Figure 1) will lead to weak co-polarization conversions, and negligible cross-polarization conversions. There will also be some weak "cavity effect" in this two-layer structure depending on the separation between layers, as shown in Figure S3. However, the 45° orientated middle grating works as an efficient polarization conversion layer to generate cross-polarization transmission. Furthermore, such a conversion mechanism is enhanced by the cavity effect within the metasurface, which leads to its broadband asymmetric light transmission behavior.

Indeed, generating asymmetric transmission for linear polarization requires anisotropic electric and bianisotropic responses (i.e. magneto-electric coupling). An arbitrary electric response can be generated using a single layer patterned sheet. However, a single sheet cannot generate magnetic and magneto-electric responses, which are necessary for a high-efficiency polarization conversion. In fact, the fundamental limit for cross-polarization conversion is 25% if only an electric response is utilized [42]. Therefore, we turn our attention to designs consisting of multiple layers. A systematic design method for realizing arbitrary polarization conversion is outlined in Ref. [32]. It is shown that each sheet can be homogenized as an

equivalent sheet impedance with well-defined transmission and reflection coefficients. This allows the overall response of multiple cascaded sheets to be calculated, which simplifies the design procedure. It can be shown that at least 3 sheets are required to independently control electric and magnetic responses [43].

In the work, we demonstrate that rather than designing complicated patterns that closely approach the ideal sheets, a simplified design with 1D metallic gratings can also achieve a relatively high performance. Consider two half-spaces separated by the metasurface, where the electric fields on either side of the metasurface are related by the following relation:

$$\begin{pmatrix} E_t^x \\ E_t^y \end{pmatrix} = \begin{pmatrix} t_{xx} & t_{xy} \\ t_{yx} & t_{yy} \end{pmatrix} \begin{pmatrix} E_i^x \\ E_i^y \end{pmatrix} = T \begin{pmatrix} E_i^x \\ E_i^y \end{pmatrix}$$

Here, T is the Jones matrix of the metasurface, and $E_i^{x/y}$ and $E_t^{x/y}$ are the incident and transmitted electric field polarized along the x and y directions, respectively. The element t_{nm} in the Jones matrix denotes transmission coefficient of the m-polarized electric field to the n-polarized electric field, and is usually a complex number (containing both field transmission amplitude and phase information). The transmission intensity coefficient T_{nm} equals the square of $|t_{nm}|$. For an ideal asymmetric transmitting device for linearly polarized light that allows unity conversion of x-polarized light to y-polarized light in one direction only, the Jones

matrix is written as: $\mathrm{T} = e^{-i\emptyset}\begin{pmatrix} 0 & 0 \\ 1 & 0 \end{pmatrix}$ [44]. For the structure in this study, its Jones matrix at 1.5 μm is calculated as $\begin{pmatrix} 0.126e^{i75.1^\circ} & 0.018e^{-i131^\circ} \\ 0.920e^{-i44.6^\circ} & 0.169e^{i51.9^\circ} \end{pmatrix}$, which approaches the ideal case. It has been recently demonstrated that by designing each layer with complex geometries, the metasurface performance can be further optimized [29, 32]. However, the design here, with only three layers of nano-gratings, is advantageous due to its simplicity and suitability for large area device fabrication, with a very minimal compromise of its performance.

The measured and simulated transmittance is plotted in Figures 4a (linear scale) and 4b (logarithmic scale), showing close correspondence. The metasurface has an averaged transmission efficiency of 80% around 1.5 μm, and an extinction ratio of 24 (13.8 dB). Due to the limited output wavelength range from the laser, the device is only characterized over a narrow band. However, numerical simulation predicts its broad operational bandwidth (FWHM bandwidth of 1.7 μm). To demonstrate this, the metasurface is also characterized using a different experimental setup consisting of a rotating analyzer spectroscopic ellipsometer (Model V-VASE, J.A. Woollam Co., Inc.) between 1200 nm and 1850 nm. The illumination beam size from the ellipsometer (about 700 μm in diameter) is much larger than the metasurface area (250 μm by 250 μm square), and the measured Jones Matrix represents a superposition of the fraction of the light beam sampling the device and the surrounding area. However, since the cross-polarization conversion only takes place within the metasurface, the

T_{xy} and T_{yx} components can be obtained. Figure 5 plots the simulated and measured T_{xy} and T_{yx} components. As the contributions from the device and surrounding area are not separated, the experimental values in Figure 5 are normalized to the simulation result at 1610 nm and are in arbitrary units. The measurement demonstrates that the device behavior corresponds well with simulation over a large bandwidth. It should be noted that, due to the absorption in a fiber optic cable on the source side of the ellipsometer, there is insufficient light intensity near 1400 nm, causing the gap in the data seen there. More accurate measurements could be ascertained by using a smaller beam spot or a series of measurements of different size beam spots to appropriately quantify the Jones matrix elements for the device area only.

A visual demonstration that highlights the performance of the metasurface is shown in Figures 4c and 4d. Figure 4c is a picture of the metasurface taken with an infrared camera when a 1.5 μm laser beam illuminates the back of the metasurface. Figure 4d corresponds to the same setup but with the metasurface flipped around so that the laser beam illuminates from the opposite side. The same laser beam intensity and polarization are maintained in the two cases. The metasurface provides high and low transmission in Figures 4c and 4d, respectively.

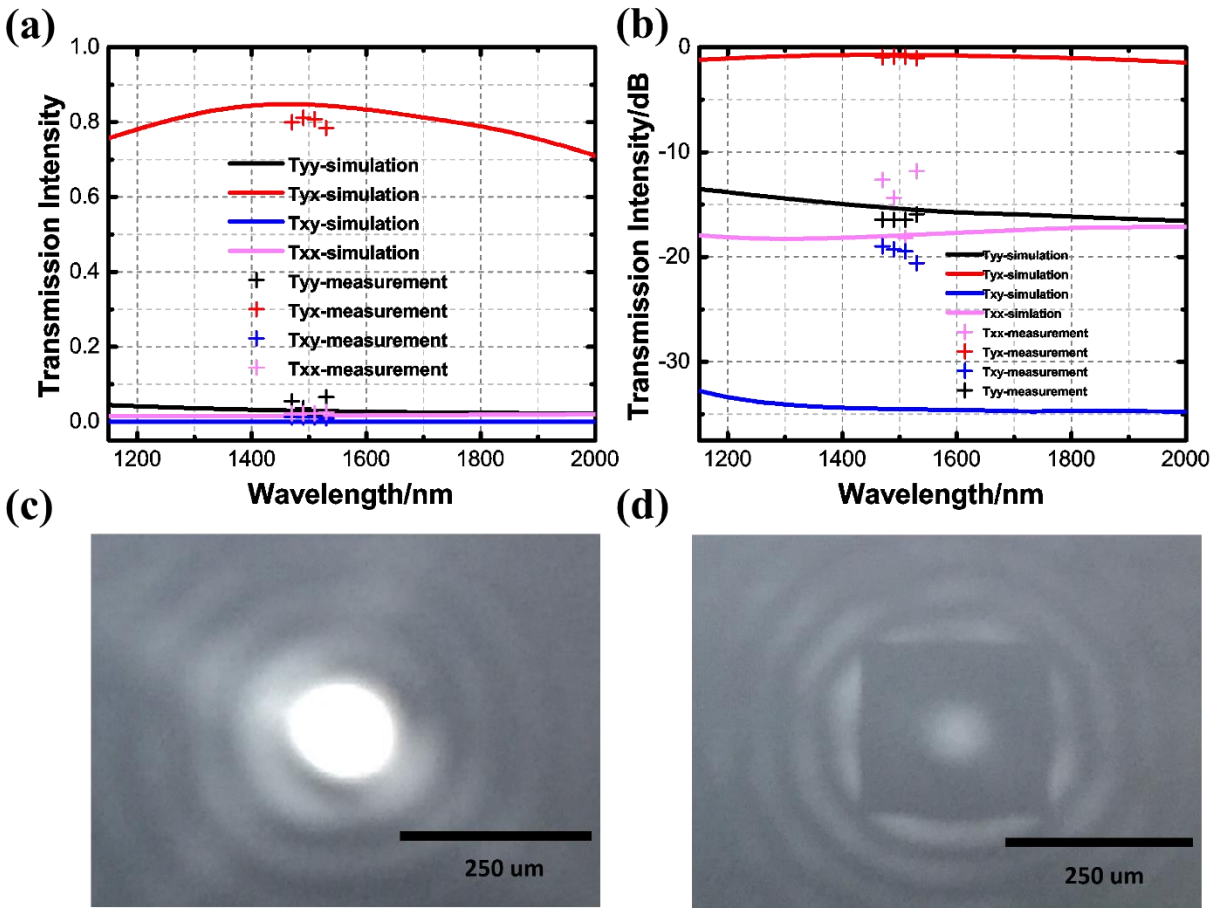

Figure 4: (a-b) Measured transmission intensity from the metasurface in linear (a) and logarithmic (b) scale; (c) Bright transmitted light pattern from one direction; (d) Blocked transmitted light pattern from the reverse direction. The incident laser beam intensity is kept the same in two cases.

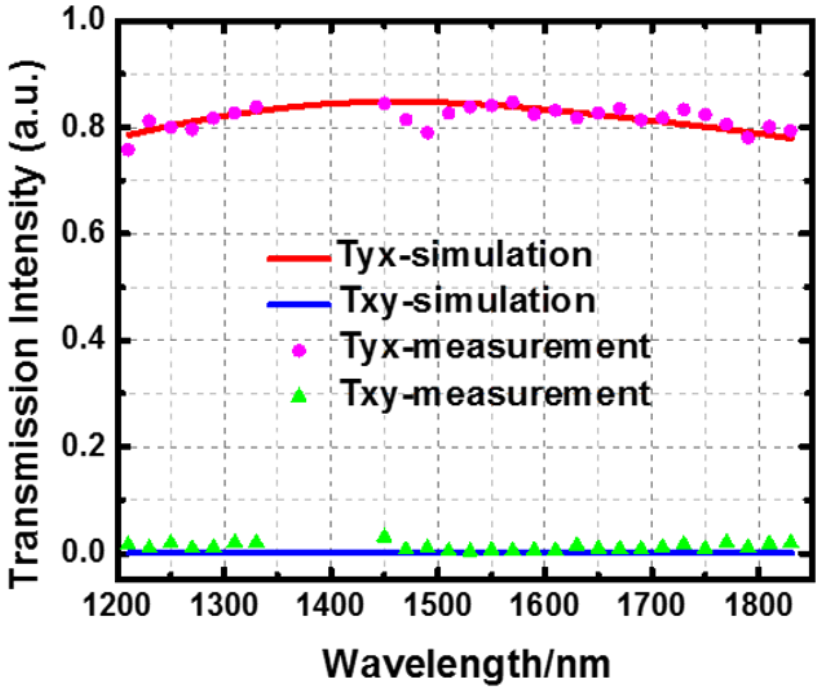

Figure 5: Measured T_{xy} and T_{yx} components with a broadband ellipsometer and large beam size. The measurement demonstrates that the device broadband behavior corresponds well with simulation.

3. Discussion

For many practical applications, the device performance should be robust to the variations in the angle of incidence [27]. This also helps reduce the requirements of other optical components in the system. Figures 6a and 6b plot the simulated transmittance of the metasurface at 1.5 μm versus different angles of incidence in the XZ and YZ plane. There is minimal performance degradation until the incident angle reaches 50^{o}. As experimental

verification, the transmittance was measured at a 30^{o} input angle (XZ and YZ plane respectively). To measure the device transmission at a 30˚ angle of incidence, the metasurface is tilted at 30˚ with respect to the input single mode fiber, and the other components in the measurement set-up are kept the same. The measurement result is plotted in Figures 6c and 6d. It can be seen that at such an incident angle, the metasurface still maintains its properties of high transmission, broad bandwidth, and good extinction ratio. The device's robust angular tolerance can be understood by examining the angular response of individual layers. Figure S4 plots the optical field reflection/transmission amplitude and phase coefficients of a single nano-grating layer at normal incidence and 30˚ angle incidence (in both XZ and YZ planes). It can be seen that the response from a single layer has a good angular tolerance and this contributes to the device's performance robustness against the angle of incidence.

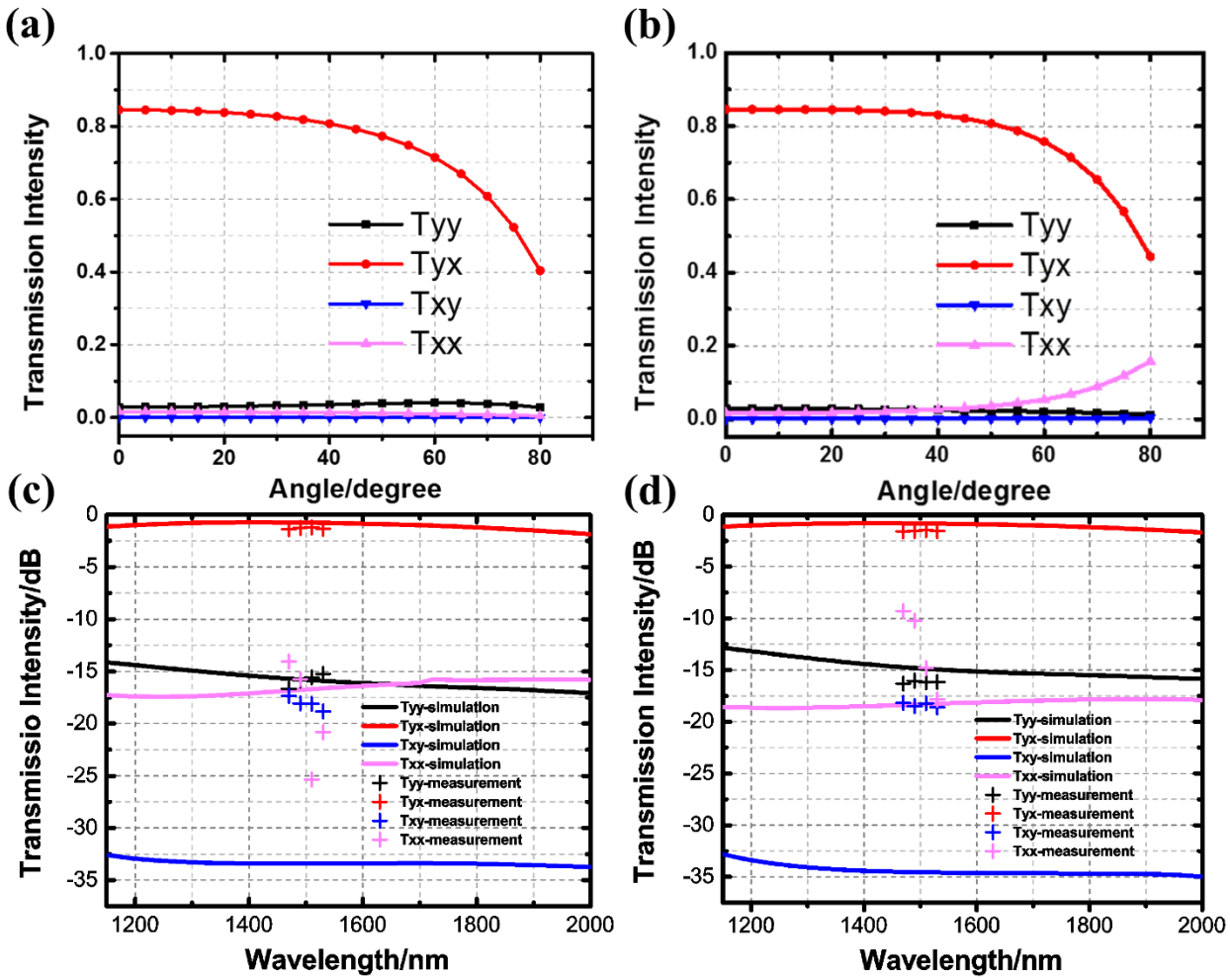

Figure 6: (a-b) Simulated transmittance at a wavelength of 1.5 μm with input light angle in the XZ (a) and YZ (b) plane; (c-d) Measured transmittance with 30 degree incident light angle in the XZ (c) and YZ (d) plane.

The metasurface performance is also insensitive to variations in the grating height, width, and period. Increasing or decreasing the grating width by 20 nm does not degrade its performance (Figure S6 in Supporting Information). Similarly, varying the grating height

(from 30 nm to 60 nm) will not affect the device performance obviously either (Figure S7 in the Supporting Information). Every individual layer functions as a linear polarizer (anisotropic element), and its anisotropic response will not change significantly with grating width variations over a certain range (Figure S5 in the Supporting Information). In other words, these three layers of cascaded Au nano-gratings can be generalized as three layers of coupled anisotropic metallic sheets (Figure 7a). This response also suggests that the nano-grating period can be modified without sacrificing device performance. As shown in Figure 7b, the transmittance of the metasurface consisting of three identical layers of 40 nm thick, 70 nm wide, and 140 nm period Au nano-gratings is plotted, and is very similar to that of three layers of Au nano-gratings with a unique middle layer grating period in Figure 4a (calculation details in the Supporting Information). Such a relaxation of the requirements on grating geometries (e.g., width and period) paves the way to realize large area device fabrication for practical applications. It is true that sub-wavelength structures are usually fabricated through electron beam lithography, which is time consuming and makes it difficult to achieve large area devices. However, for certain structures such as the nano-gratings in this study, they can be easily realized by various methods such as interference lithography [45], plasmonic lithography [46, 47], or nano-imprinting [48, 49]. The insensitivities of the device performance to variations in the grating geometry leave room for reasonable fabrication errors/inaccuracies.

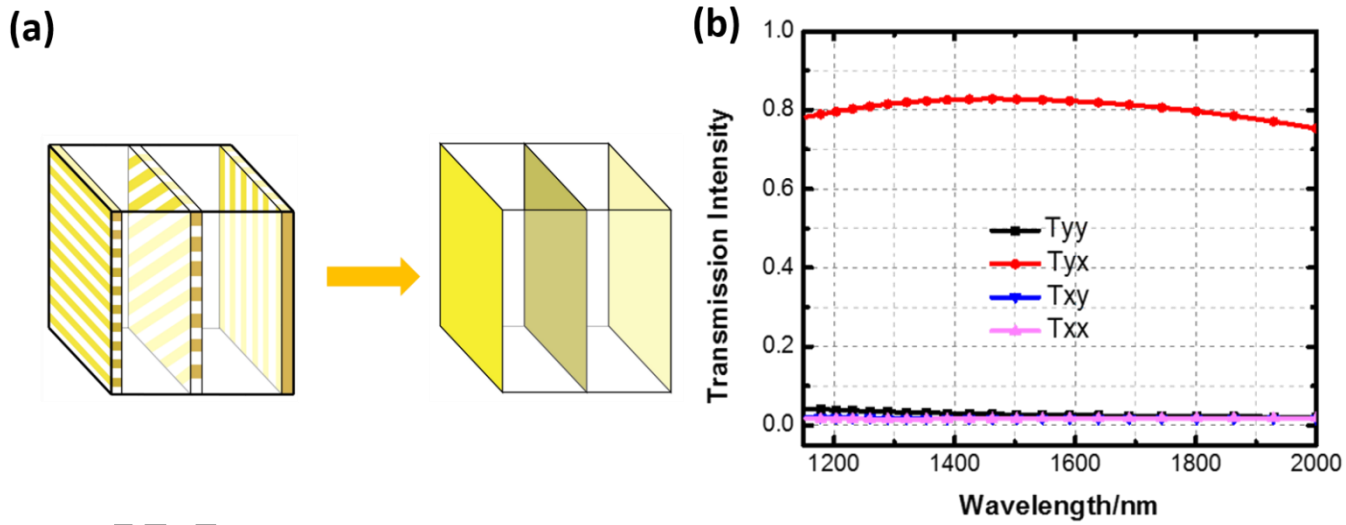

Figure 7: (a) Generalized model of the metasurface as coupled metallic sheets; (b) Simulated transmittance of metasurface with three layers of identical Au nano-gratings.

Further, the design strategy for the metasurface can be easily extended to other wavelength ranges to achieve asymmetric light transmission devices. One simple way is to modify the spacer layer thickness. As shown in Figure S8 in the Supporting Information, asymmetric light transmission centered at 1 μm and 2 μm can be realized by setting the spacer thickness as 70 nm and 260 nm respectively. Moving the current design with Gold to the visible regime will lead to a degraded performance, because of the high optical loss with Gold in this wavelength range. We believe better designs can be achieved by choosing low loss constituent materials (e.g., Silver or Aluminum) [50], and engineering the geometry of the constituent layers in order to achieve impedance matching with air and therefore, a suppressed reflection.

5. Conclusions and Outlook

In summary, a thin (λ/5) asymmetric light transmitting metasurface is designed and experimentally demonstrated. It has the advantages of high transmission (80%), broad bandwidth (FWHM bandwidth of 1.7 μm), and good extinction ratio (24; 13.8 dB). In addition, its performance is insensitive to both the incident light angle and the constituent nano-structure geometric variations. A comparison between the metasurface in this work and recently reported structures is listed in Table S1 in the Supporting Information, where the metasurface in this study shows a comparable or better performance in terms of the bandwidth, efficiency, and foot print. Furthermore, the design principle is general and can be applied to other wavelength ranges. In addition, the device structure is suitable for large area device manufacturing techniques such as a nano-imprinting or roll-to-roll printing.

Supporting Information:

Numerical simulations (including calculated transmission through three layers of Au nano-wires based on the Malus' law and simulated response from the metasurface); Response of individual nano-grating layer with different angle of incidence and grating width; Metasurface response with varying nano-grating width and height; Asymmetric light transmission at other wavelength ranges. Comparison between the asymmetric light transmitting metasurface in this work and recently reported structures. Additional supporting information may be found in the online version of this article at the publisher's website.

Acknowledgements:

This work is supported by the NSF Materials Research Science and Engineering Center (MRSEC) Program DMR 1120923. The authors acknowledge the technical support from the Lurie Nanofabrication Facility (LNF) at the University of Michigan. C. Zhang acknowledges discussions with Dr. Young Jae Shin, Dr. Tao Ling, and Mr. Chengang Ji.

Received: ((will be filled in by the editorial staff))
Revised: ((will be filled in by the editorial staff))
Published online: ((will be filled in by the editorial staff))

Keywords: asymmetric light transmission, metasurface, metamaterial, angle-insensitive device, plasmonics

References:

[1] J. Y. Chin, T. Steinle, T. Wehlus, D. Dregely, T. Weiss, V. I. Belotelov, et al., "Nonreciprocal plasmonics enables giant enhancement of thin-film Faraday rotation," Nature Communications, vol. 4, p. 1599, 2013.

[2] J. L. O'Brien, G. J. Pryde, A. G. White, T. C. Ralph, and D. Branning, "Demonstration of an all-optical quantum controlled-NOT gate," Nature, vol. 426, pp. 264-267, 2003.

[3] E. Knill, R. Laflamme, and G. J. Milburn, "A scheme for efficient quantum computation with linear optics," Nature, vol. 409, pp. 46-52, 2001.

[4] R. Fleury, D. L. Sounas, C. F. Sieck, M. R. Haberman, and A. Alù, "Sound Isolation and Giant Linear Nonreciprocity in a Compact Acoustic Circulator," Science, vol. 343, pp. 516-519, 2014.

[5] R. Singh, E. Plum, C. Menzel, C. Rockstuhl, A. K. Azad, R. A. Cheville, et al., "Terahertz metamaterial with asymmetric transmission," Physical Review B, vol. 80, p. 153104, 2009.

[6] S. Cakmakyapan, A. E. Serebryannikov, H. Caglayan, and E. Ozbay, "Spoof-plasmon relevant one-way collimation and multiplexing at beaming from a slit in metallic grating," Optics Express, vol. 20, pp. 26636-26648, 2012.

[7] C. Menzel, C. Helgert, C. Rockstuhl, E. B. Kley, A. Tünnermann, T. Pertsch, et al., "Asymmetric Transmission of Linearly Polarized Light at Optical Metamaterials," Physical Review Letters, vol. 104, p. 253902, 2010.

[8] V. A. Fedotov, A. S. Schwanecke, N. I. Zheludev, V. V. Khardikov, and S. L. Prosvirnin, "Asymmetric Transmission of Light and Enantiomerically Sensitive Plasmon Resonance in Planar Chiral Nanostructures," Nano Letters, vol. 7, pp. 1996-1999, 2007.

[9] D. Jalas, A. Petrov, M. Eich, W. Freude, S. Fan, Z. Yu, et al., "What is and what is not an optical isolator," Nature Photonics, vol. 7, pp. 579-582, 2013.

[10] L. Bi, J. Hu, P. Jiang, D. H. Kim, G. F. Dionne, L. C. Kimerling, et al., "On-chip optical isolation in monolithically integrated non-reciprocal optical resonators," Nature Photonics, vol. 5, pp. 758-762, 2011.

[11] A. Cicek, M. B. Yucel, O. A. Kaya, and B. Ulug, "Refraction-based photonic crystal diode," Optics Letters, vol. 37, pp. 2937-2939, 2012.

[12] C. Wang, X.-L. Zhong, and Z.-Y. Li, "Linear and passive silicon optical isolator," Scientific Reports, vol. 2, 2012.

[13] J. K. Gansel, M. Thiel, M. S. Rill, M. Decker, K. Bade, V. Saile, et al., "Gold Helix Photonic Metamaterial as Broadband Circular Polarizer," Science, vol. 325, pp. 1513-1515, 2009.

[14] T. Xu and H. J. Lezec, "Visible-frequency asymmetric transmission devices incorporating a hyperbolic metamaterial," Nature Communications, vol. 5, 2014.

[15] S. Wu, S. Xu, Y. Zhang, Y. Wu, J. Jiang, Q. Wang, et al., "Asymmetric transmission and optical rotation of a quasi-3D asymmetric metallic structure," Optics Letters, vol. 39, pp. 6426-6429, 2014.

[16] F. Qin, L. Ding, L. Zhang, F. Monticone, C. C. Chum, J. Deng, et al., "Hybrid bilayer plasmonic metasurface efficiently manipulates visible light," Science Advances, vol. 2, 2016.

[17] Z. Li, S. Chen, C. Tang, W. Liu, H. Cheng, Z. Liu, et al., "Broadband diodelike asymmetric transmission of linearly polarized light in ultrathin hybrid metamaterial," Applied Physics Letters, vol. 105, p. 201103, 2014.

[18] S. Cakmakyapan, H. Caglayan, A. E. Serebryannikov, and E. Ozbay, "Experimental validation of strong directional selectivity in nonsymmetric metallic gratings with a subwavelength slit," Applied Physics Letters, vol. 98, p. 051103, 2011.

[19] S. Cakmakyapan, A. E. Serebryannikov, H. Caglayan, and E. Ozbay, "One-way transmission through the subwavelength slit in nonsymmetric metallic gratings," Optics Letters, vol. 35, pp. 2597-2599, 2010.

[20] Z. H. Zhu, K. Liu, W. Xu, Z. Luo, C. C. Guo, B. Yang, et al., "One-way transmission of linearly polarized light in plasmonic subwavelength metallic grating cascaded with dielectric grating," Optics Letters, vol. 37, pp. 4008-4010, 2012.

[21] A. E. Minovich, A. E. Miroshnichenko, A. Y. Bykov, T. V. Murzina, D. N. Neshev, and Y. S. Kivshar, "Functional and nonlinear optical metasurfaces," Laser & Photonics Reviews, vol. 9, pp. 195-213, 2015.

[22] N. Yu and F. Capasso, "Flat optics with designer metasurfaces," Nature Materials, vol. 13, pp. 139-150, 2014.

[23] Y. Nanfang, P. Genevet, F. Aieta, M. A. Kats, R. Blanchard, G. Aoust, et al., "Flat Optics: Controlling Wavefronts With Optical Antenna Metasurfaces," Selected Topics in Quantum Electronics, IEEE Journal of, vol. 19, pp. 4700423-4700423, 2013.

[24] A. V. Kildishev, A. Boltasseva, and V. M. Shalaev, "Planar Photonics with Metasurfaces," Science, vol. 339, March 15, 2013 2013.

[25] C. Pfeiffer and A. Grbic, "Metamaterial Huygens' Surfaces: Tailoring Wave Fronts with Reflectionless Sheets," Physical Review Letters, vol. 110, p. 197401, 2013.

[26] H. Cheng, Z. Liu, S. Chen, and J. Tian, "Emergent Functionality and Controllability in Few-Layer Metasurfaces," Advanced Materials, pp. 5410–5421, 2015.

[27] Y.-K. R. Wu, A. E. Hollowell, C. Zhang, and L. J. Guo, "Angle-Insensitive Structural Colours based on Metallic Nanocavities and Coloured Pixels beyond the Diffraction Limit," Scientific Reports, vol. 3, 2013.

[28] A. Shaltout, J. Liu, V. M. Shalaev, and A. V. Kildishev, "Optically Active Metasurface with Non-Chiral Plasmonic Nanoantennas," Nano Letters, vol. 14, pp. 4426-4431, 2014.

[29] C. Pfeiffer, C. Zhang, V. Ray, L. J. Guo, and A. Grbic, "High Performance Bianisotropic Metasurfaces: Asymmetric Transmission of Light," Physical Review Letters, vol. 113, p. 023902, 2014.

[30] Y. Yang, W. Wang, P. Moitra, I. I. Kravchenko, D. P. Briggs, and J. Valentine, "Dielectric Meta-Reflectarray for Broadband Linear Polarization Conversion and Optical Vortex Generation," Nano Letters, vol. 14, pp. 1394-1399, 2014.

[31] N. K. Grady, J. E. Heyes, D. R. Chowdhury, Y. Zeng, M. T. Reiten, A. K. Azad, et al., "Terahertz Metamaterials for Linear Polarization Conversion and Anomalous Refraction," Science, vol. 340, pp. 1304-1307, 2013.

[32] C. Pfeiffer and A. Grbic, "Bianisotropic Metasurfaces for Optimal Polarization Control: Analysis and Synthesis," Physical Review Applied, vol. 2, p. 044011, 2014.

[33] C. Pfeiffer, C. Zhang, V. Ray, L. Jay Guo, and A. Grbic, "Polarization rotation with ultra-thin bianisotropic metasurfaces," Optica, vol. 3, pp. 427-432, 2016.

[34] D. Lin, P. Fan, E. Hasman, and M. L. Brongersma, "Dielectric gradient metasurface optical elements," Science, vol. 345, pp. 298-302, 2014.

[35] X. Ni, S. Ishii, A. V. Kildishev, and V. M. Shalaev, "Ultra-thin, planar, Babinet-inverted plasmonic metalenses," Light Sci Appl, vol. 2, p. e72, 2013.

[36] C. Pfeiffer, N. K. Emani, A. M. Shaltout, A. Boltasseva, V. M. Shalaev, and A. Grbic, "Efficient Light Bending with Isotropic Metamaterial Huygens' Surfaces," Nano Letters, vol. 14, pp. 2491-2497, 2014.

[37] C. Pfeiffer and A. Grbic, "Controlling Vector Bessel Beams with Metasurfaces," Physical Review Applied, vol. 2, p. 044012, 2014.

[38] P. R. West, J. L. Stewart, A. V. Kildishev, V. M. Shalaev, V. V. Shkunov, F. Strohkendl, et al., "All-dielectric subwavelength metasurface focusing lens," Optics Express, vol. 22, pp. 26212-26221, 2014.

[39] R. Czaplicki, H. Husu, R. Siikanen, J. Mäkitalo, M. Kauranen, J. Laukkanen, et al., "Enhancement of Second-Harmonic Generation from Metal Nanoparticles by Passive Elements," Physical Review Letters, vol. 110, p. 093902, 2013.

[40] J. A. H. van Nieuwstadt, M. Sandtke, R. H. Harmsen, F. B. Segerink, J. C. Prangsma, S. Enoch, et al., "Strong Modification of the Nonlinear Optical Response of Metallic Subwavelength Hole Arrays," Physical Review Letters, vol. 97, p. 146102, 2006.

[41] G. Li, S. Chen, N. Pholchai, B. Reineke, P. W. H. Wong, E. Y. B. Pun, et al., "Continuous control of the nonlinearity phase for harmonic generations," Nature Materials, vol. 14, pp. 607-612, 2015.

[42] F. Monticone, N. M. Estakhri, and A. Alù, "Full Control of Nanoscale Optical Transmission with a Composite Metascreen," Physical Review Letters, vol. 110, p. 203903, 2013.

[43] C. Pfeiffer and A. Grbic, "Millimeter-Wave Transmitarrays for Wavefront and Polarization Control," IEEE Transactions on Microwave Theory and Techniques, vol. 61, pp. 4407-4417, 2013.

[44] C. Menzel, C. Rockstuhl, and F. Lederer, "Advanced Jones calculus for the classification of periodic metamaterials," Physical Review A, vol. 82, p. 053811, 2010.

[45] C. Lu and R. H. Lipson, "Interference lithography: a powerful tool for fabricating periodic structures," Laser & Photonics Reviews, vol. 4, pp. 568-580, 2010.

[46] X. Chen, F. Yang, C. Zhang, J. Zhou, and L. J. Guo, "Large-Area High Aspect Ratio Plasmonic Interference Lithography Utilizing a Single High-k Mode," ACS Nano, vol. 10, pp. 4039-4045, 2016.

[47] W. Srituravanich, N. Fang, C. Sun, Q. Luo, and X. Zhang, "Plasmonic Nanolithography," Nano Letters, vol. 4, pp. 1085-1088, 2004.

[48] C. Zhang, H. Subbaraman, Q. Li, Z. Pan, J. G. Ok, T. Ling, et al., "Printed photonic elements: nanoimprinting and beyond," Journal of Materials Chemistry C, 4, pp. 5133-5153, 2016.

[49] L. J. Guo, "Nanoimprint Lithography: Methods and Material Requirements," Advanced Materials, vol. 19, pp. 495-513, 2007.

[50] C. Zhang, D. Zhao, D. Gu, H. Kim, T. Ling, Y.-K. R. Wu, et al., "An Ultrathin, Smooth, and Low-Loss Al-Doped Ag Film and Its Application as a Transparent Electrode in Organic Photovoltaics," Advanced Materials, vol. 26, pp. 5696-5701, 2014.